Application of GSA/GLUE methods to evaluate the representation of suspended sediment transport during flash floods in a rainfall-runoff model

Atiyeh Hosseinzadeh, Hélène Roux, Ludovic Cassan, Audrey Douinot

Available online at www.sciencedirect.com

ScienceDirect

IFAC PapersOnLine 55-5 (2022) 90–95

Application of GSA/GLUE methods to evaluate the representation of suspended sediment transport during flash floods in a rainfall-runoff model

A. Hosseinzadeh*, H. Roux*, L. Cassan*, and A. Douinot**

** Institut de Mécanique des Fluides de Toulouse (IMFT), Université de Toulouse, CNRS, Toulouse, France (e-mail : atiyeh.hosseinzade@toulouse-inp.fr, Helene.Roux@imft.fr, Ludovic.Cassan@imft.fr).*

*** Luxembourg Institute of Science and technology (LIST), ERIN, Luxembourg (e-mail: audreydouinot@gmail.com)*

Abstract: This study looks at the impact of different parameters involved in the simulation of suspended sediment transport during flash flood on the performances of a distributed event-based soil erosion model. The results of GSA/GLUE methodologies implemented on three flash flood events show the model sensitivity to two parameters: the coefficient of soil sensitivity to shear erosion and the median diameter of sediment particles. The need to take into account the spatial variability of this soil sensitivity to shear erosion and therefore the location of potential sources of sediment is also stressed.

Keywords: flash flood, suspended sediment transport, soil erosion, sensitivity analysis, GLUE

1. INTRODUCTION

Understanding the dynamic of suspended sediment transport during flash floods is an essential step to forecast and manage the consequences of these events. Several formulations, either empirical or physically-based have been proposed to represent these phenomena (Merritt et al., 2003; Aksoy and Kavvas, 2005). Physically-based models often require an extensive database whereas empirical ones involve parameters that are difficult to quantify and for which no a priori estimates are available. The number of parameters, their spatial and temporal variabilities but also the respective uncertainties of these representations will increase the difficulty of calibration of the model. This emphasis the need to identify the parameters which have the highest impact on the model response and as a result helps to limit the number of parameters to calibrate but also to reduce the uncertainty on the model outputs. Hornberger and Spear (1981) created regional sensitivity analysis (RSA), which was later renamed generalized sensitivity analysis (GSA) by Freer et al. (1996) in the context of environmental modeling. Studying uncertainty sources is a popular issue in hydrology which can be accomplished using a variety of methods, the most popular of which are formal Bayesian methods (Kuczera and Parent 1998) and the generalized likelihood uncertainty estimation (GLUE) method (Beven and Binley 1992), as well as recursive application of GSA for dynamic identifiability analysis (Wagener et al. 2003) or Bayesian total error analysis (Kavetski et al. 2006).

The aim of this paper is to study the impacts of parameters involved in soil erosion modelling during flash floods on the response of a dedicated model using GSA and GLUE methodologies. The chosen model is a physically-based model but with a parsimonious parameterization taking advantage of existing databases.

The methodology is described in §2, including the presentation of the test site and available data, the rainfall-runoff model, the suspended sediment transport model and the calibration process. §3 describes the results, both in terms of model performances and sensitivity and uncertainty analysis on three flood events. §4 summarizes the key facts and proposes some perspectives.

2. METHODOLOGY

2.1 Study zone and available data

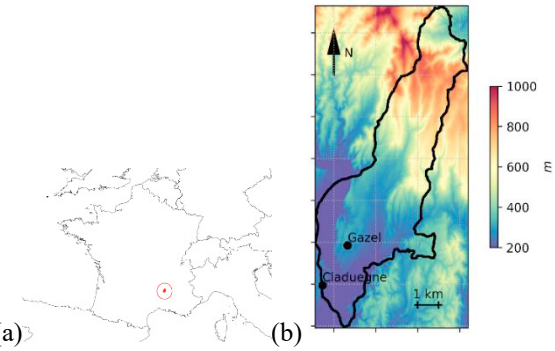

Figure 1. Study zone: (a) Location of the Cladueègne catchment (b) 1m DEM derived from an aerial lidar dataset acquired in 2012 and processed by Sintégra (Braud et al., 2014), provided by (Nord et al., 2017))

The study site is the Cladueegne catchment (42.3 km^2) which is a research catchment in south of France and a part of OHMCV observatory in OZCAR-RI sites (Gaillardet et al., 2018).

Cladueegne in terms of geology is divided into two separate sections including: basaltic components in northern part and clay and limestone in southern one. The range of elevation varies from approximately 230 m to 820 m from the outlet towards the highest point of the catchment (Fig. 1). This catchment has an oceanic and Mediterranean climate with heavy rainfall and flash floods in autumn. Main land use types are pastures, vineyards and forest (Uber, 2020).

10.1016/j.ifacol.2022.07.645

The data used for implementing the model include rainfall, topography, soil properties, land use and continuous discharge and are available in Nord et al. (2017). Turbidity data are collected by the Hydrology Observatory Database (BDOH) (Didon-Lescot, J.-F, et al., 2015) and suspended sediment concentrations (SSC) is estimated using a T-SSC rating curve as in Uber (2020).

2.2 Hydrodynamic model

The MARINE model is a distributed mechanistic hydrological model specially developed for flash-flood simulations and including a soil erosion model. MARINE is a physically based model structured in three main modules. The first module is used to have a ratio of surface runoff and infiltration from the rainfall, the second one addresses the subsurface downhill flow, and the third one represents the overland and channel flows. By using Saint-Venant equations, the transfer function component can convey the rainfall excess to the catchment outlet. The Digital Elevation Model grid resolution, which is a regular grid of squares cells, is used to spatially discretize the watershed. Evapotranspiration can be negligible at the time scale of flash flood events (Roux, 2011).

The model calibration is based on sensitivity procedure, which is described in section 2.4.

2.3 Soil erosion model

The time and spatial evolution of suspended sediment concentration is computed from the depth-averaged scalar transport equation including source terms to account for the production and deposition of suspended sediment (Eq. 1). The soil is composed of a layer of erodible particles represented by their median diameter. The net sediment flux $(E-D)$ will be determined by the model of concentration at equilibrium according to van Rijn (1984). A term of rainfall-driven detachment rate D_r based on Wicks and Bathurst (1996) is added as suggested by Cea et al. (2016) (Eq. 2).

$$\frac{\partial(hC)}{\partial t}+\frac{\partial(hUC)}{\partial x}=E-D+D_r \quad (1)$$

$$D_r=\frac{k_r}{\rho_s}F_w KE \quad (2)$$

Where C is concentration (mass fraction) [-], h is water depth $[m]$, U is velocity $[m.\ s^{-1}]$, $E-D$ is net sediment flux $[m.\ s^{-1}]$ and D_r raindrop erosion rate $[m.s^{-1}]$.
Raindrop erosion rate is related to k_r which is an erodibility coefficient $[kg^{-1}.m^{-2}.s^2]$, F_w water depth correction factor [-], and KE kinematic energy of precipitation $[(kg.m.s^{-1}).m^{-2}.s^{-1}]$ (Wicks and Bathurst, 1996).
Water depth correction factor (F_w) is linked to water depth (h) and raindrop diameter (d_{pluie}) (Eq. 3).

$$F_w=\begin{cases} exp\left(1-\dfrac{h}{d_{pluie}}\right) & if\ h>d_{pluie} \\ 1 & otherwise \end{cases} \quad (3)$$

The raindrop diameter is calculated based on I_{pluie} which is rainfall intensity $[mm.h^{-1}]$ (Eq. 4).

$$d_{pluie}=0.00124{I_{pluie}}^{0.182} \quad (4)$$

The assumption of a non-linear relationship between kinematic energy of rainfall and rainfall intensity is made as follow (Eq. 5):

$$KE=\alpha {I_{pluie}}^{\beta} \quad (5)$$

α and β are empirical coefficients that vary with rainfall intensity. Corresponding values can be found in Wicks and Bathurst (1996). k_r is estimated from experimental data and describes the ease of detachment by raindrop, so qualitatively it is expected to increase from clay, through silt, to sand soil. Mean values of k_r for different soil texture are also presented in Wicks and Bathurst (1996).
Therefore, the soil erosion model relies on four main parameters:

- $d_{50}\ [m]$ the median diameter of sediment particle involved in the calculation of the net sediment flux $(E-D)$ (van Rijn, 1984),
- $Z_{ref}\ [m]$ the location of the interface between bed load and suspended load which is used in the calculation of the net sediment flux $(E-D)$ (van Rijn, 1984),
- $FSE\ [-]$ the coefficient of soil sensitivity to shear erosion which is also involved in the calculation of the net sediment flux $(E-D)$ (van Rijn, 1984) and represents the ratio between effective and total shear stresses as follow (Eq. 6):

$$FSE=\frac{\tau_p}{\rho g h I} \quad (6)$$

  Where τ_p is the shear stress $[kg.m^{-1}.s^{-2}]$ which is computed independently of the sediment concentration by the hydrodynamic model and related to the choice of the roughness coefficient, ρ is the water density $[kg.m^{-3}]$, g is the gravitational acceleration $[m.\ s^{-2}]$ and I is the topographic slope $[-]$,
- $k_r\ [kg^{-1}.m^{-2}.s^2]$ the coefficient of soil sensitivity to raindrop erosion (Eq. 2).

2.4 Calibration method

The calibration of the rainfall-runoff module is described in details in Garambois et al. (2015). It involves sensitivity analysis both to study the influence of each model parameter on the simulated output and to select calibration events.
The same type of methodology is applied to the soil erosion module. A sensitivity analysis is performed on the 4 parameters mentioned in §2.3: d_{50}, Z_{ref}, FSE and k_r. The ranges of variation are set apriori based on the physical significance of these parameters and previous studies such as Wicks and Bathurst (1996) and Uber (2020) (Table 1). Monte-Carlo simulations are then achieved by running the model with different randomly chosen sets of parameter values. Each set of parameter values is assigned a likelihood of being a simulator of the system, on the basis of the chosen likelihood measure.
The sensitivity of the model predictions to the individual parameters is assessed with the generalized sensitivity analysis (Hornberger and Spear, 1981). Distributions for each parameter are built conditioned on a classification of the Monte-Carlo simulations into two classes: behavioral and non-behavioral. A strong difference between distributions reveals

a sensitive parameter. The likelihood weights associated with behavioral simulations are applied in the Generalized Likelihood Uncertainty Estimation (GLUE) to describe the model uncertainty (Freer et al., 1996).

Table 1. Range of variation for sensitivity analysis of the soil erosion parameters

Parameter	Min	Max	Sampling
d_{50} $[mm]$	0.010	0.15	Uniform
Z_{ref} $[m]$	0.001	0.02	Uniform
FSE [-]	0.01	1	Uniform
k_r $[kg^{-1}.m^{-2}.s^2]$	0.0	100	Uniform

3. RESULT AND DISCUSSION

3.1 Model performance

Calibration of the hydrological model has been made on both Cladugne and Gazel stations (Fig. 1) using following events: 2011/11/04, 2013/05/18, 2013/10/20, 2014/01/19, 2014/10/13, 2014/11/04, 2014/11/09.
Table 2 shows the value of the calibrated parameters for the hydrodynamic part.

Table 2. Calibrated parameters for the hydrodynamic model

Parameters	Description	Value
C_z	Correction coefficient of the soil thickness [-]	0.685
C_k	Correction coefficient of the hydraulic conductivity [-]	15.1
C_{KSSz}	Correction coefficient of the soil lateral transmissivity [-]	1145
K_{kD1}	Strickler roughness coefficient of main channel $[m^{1/3}s^{-1}]$	11.2
K_{kD2}	Strickler roughness coefficient of the overbank $[m^{1/3}s^{-1}]$	18.2

Monte Carlo sample with at least 3000 members are created with uniform random generator to perform a sensitivity analysis for three flood events with different rainfall data where applicable.

The characteristics of these selected events are presented in Table 3 along with performance criteria; the NASH corresponding to the hydrodynamic simulation (NASH-H) and the NASH corresponding to the best SSC simulation among the Monte-Carlo simulations (NASH-S). In terms of hydrodynamic, the simulations are satisfactory (NASH-H≥0.8) except for Ev.3.1. It seems that for this event, the spatial variability of rainfall represented with rain gauge data (Fig. 2c) does not give satisfactory simulations as opposed to radar data (Fig. 2d). The result of the simulation based on rain gauges' data leads to clearly overestimated values of discharges. The best sediment transport simulations for all the events are reasonable (NASH-S>0.5).

Table 3. Characteristics of selected events at Cladugne (peak discharge (Q_{peak}), time of peak discharge (t_{Qpeak}), peak sediment suspended concentration (SSC_{peak}), time of that ($t_{SSCpeak}$) and simulated Nash-Sutcliffe efficiencies (NASH-H: Hydrodynamic & NASH-S: Sediment transport)

Events	2014/11/04	2014/10/10	2013/10/20	
t_{Qpeak}	11/04 14:30	10/10 23:20	10/20 10:10	
Q_{peak} $[m^3/s]$	212.5	48.3	54.6	
$t_{SSCpeak}$	11/04 14:20	10/10 23:20	10/20 10:00	
SSC_{peak} $[g/l]$	31.1	3.66	11.5	
Name	Ev.1	Ev.2	Ev.3.1	Ev.3.2
Rainfall data	gauges	gauges	gauges	radar
Cumulative rainfall $[mm]$	222.1	77.2	89.1	73.0
Runoff coefficient $[-]$	0.670	0.569	0.514	0.484
NASH-H	0.965	0.884	0.387	0.798
NASH-S	0.752	0.548	0.816	0.701

Following the recommendations of Li et al. (2010) for a relevant application of the GLUE method, a threshold value of NASH-S=0 has been chosen to ensure both simulations of concentration in the same range of variation as those observed and a statistically representative number of simulations. The number of behavioral simulations is above 300 for all events, except for Ev.2 with only 11 behavioral simulations. Due to the very low number of behavioral simulations, the results of GSA and GLUE for Ev.2 cannot be trusted. However, two remarks can be made (Fig. 3). First, SSC observations are missing during the last and highest concentration peak, which makes any analysis difficult, even for the best simulation. Secondly, it seems that the first concentration peak is largely overestimated by the simulations and arrives too early compared to the observed peak. As shown in Fig. 2b, higher rainfall intensity and most of the precipitation during Ev.2 fell on the downstream part of the catchment (south) where are located several erosion zones that are considered as potential sources of sediments by Uber (2020). The location of these

sediment sources is not included in the model, which considers a potentially diffuse erosion over the entire surface of the catchment: indeed, the values of the FSE and k_r coefficients are uniform. Fig. 5 depicts the erosion/deposition heights in each cell at the end of two events. It can be seen on Fig. 5b for Ev.2 that the erosion simulated in the southern part is not greater than that simulated in the northern part. The poor SCC results for Ev.2 seem to show that it is important to take into account the spatial variability of the erosion sensitivity in the model.

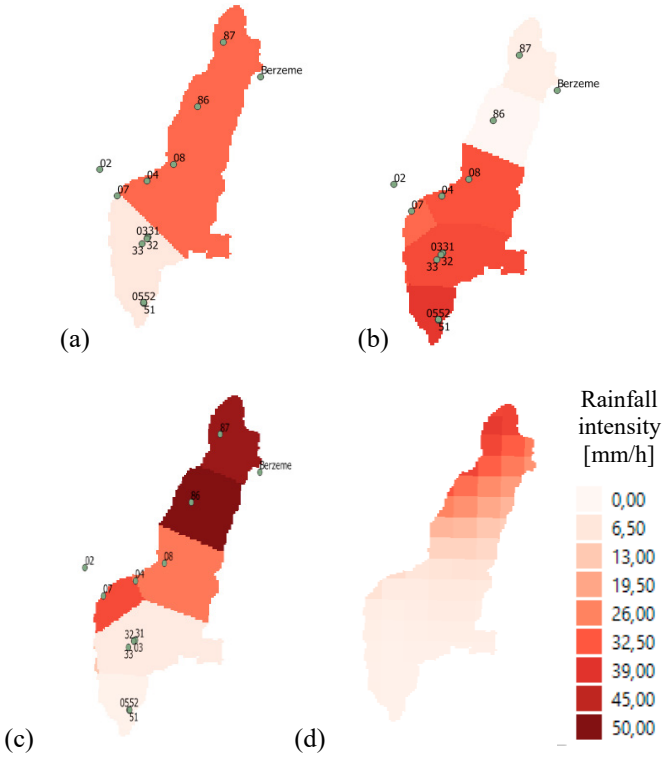

Figure 2. Intensity of precipitation at the rainfall peak for (a) Ev.1 2014/11/04 at 6:00, (b) Ev.2 2014/10/10 at 22:00, and Ev.3 2013/10/10 at 8:00 (c) Ev.3.1 based on raingauge data (d) Ev.3.2 based on radar data. Green dots and numbers correspond to the locations of raingauges.

For Ev.1, an underestimation of the SSC peak value is observed (Fig. 4). The represented spatial variability of rainfall intensity and consequently cumulative rainfall is limited due to the availability of only two raingauges for this event (Fig. 2a). It can be seen that the erosion for Ev.1 is more important on the northern part (Fig. 5a) which also presents higher rainfall intensity (Fig. 2a), whereas there are more deposits on the southern part. This simulated behavior is relevant with the observed rainfall intensity but doesn't take into account the location of the sediment sources as explained before.

3.2 Sensitivity to parameters

Table 4 illustrates the rank of each parameter based on the biggest distance between behavioral and non-behavioral distributions using the Kolmogorov-Smirnov test with more than 90% significant level for the Generalized Sensitivity

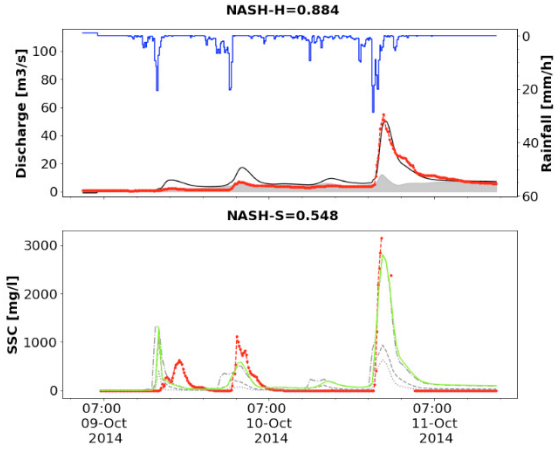

Figure 3. Ev.2 (2014/10/10). Top: Rainfall (blue), observed discharge (red dots), simulated discharge (black), subsurface flow (grey area), Bottom: observed SSC (red), best SSC simulation (green) and uncertainty interval (10, 50, 90% quantiles, dashed black)

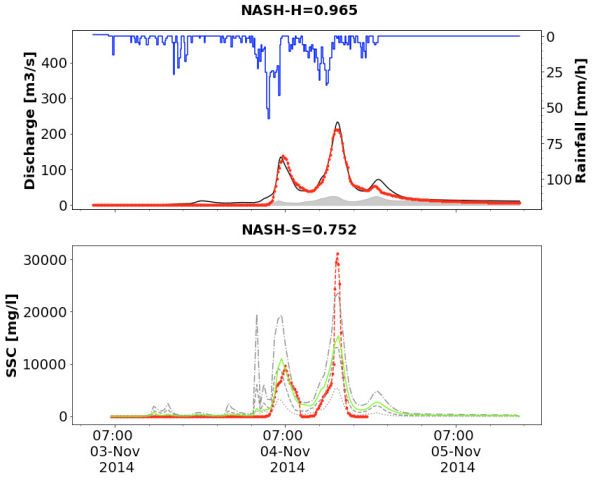

Figure 4. Ev.1 (2014/11/04). Top: Rainfall (blue), observed discharge (red dots), simulated discharge (black), subsurface flow (grey area), Bottom: observed SSC (red), best SSC simulation (green) and uncertainty interval (10, 50, 90% quantiles, dashed black)

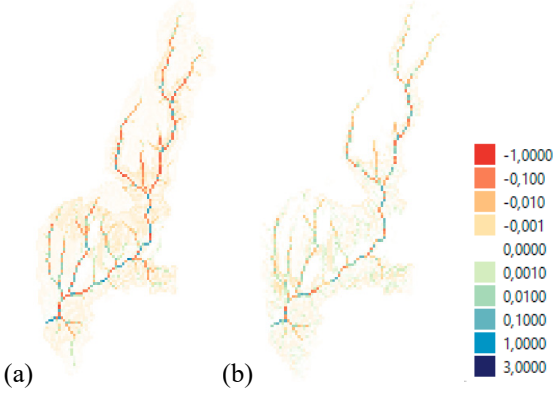

Figure 5. Map of erosion/deposition heights [m] at the end of event for (a) Ev.1 (b) Ev.2.

Analysis as proposed by Hornberger and Spear (1981). When behavioral and non-behavioral distributions are almost the same, no value is indicated in Table 4.

The results of the sensitivity analysis show that for all events FSE is the most sensitive parameter followed by d_{50}. However the results are not significant for Ev.2 because of the few behavioral simulations.

Table 4. Parameter ranking based on distance between the behavioral and non-behavioral distributions

	d_{50}	Z_{ref}	FSE	k_r
Event 1	2	*3*	1	-
Event 2	2	3	1	4
Event 3.1	2	-	1	-
Event 3.2	2	-	1	3

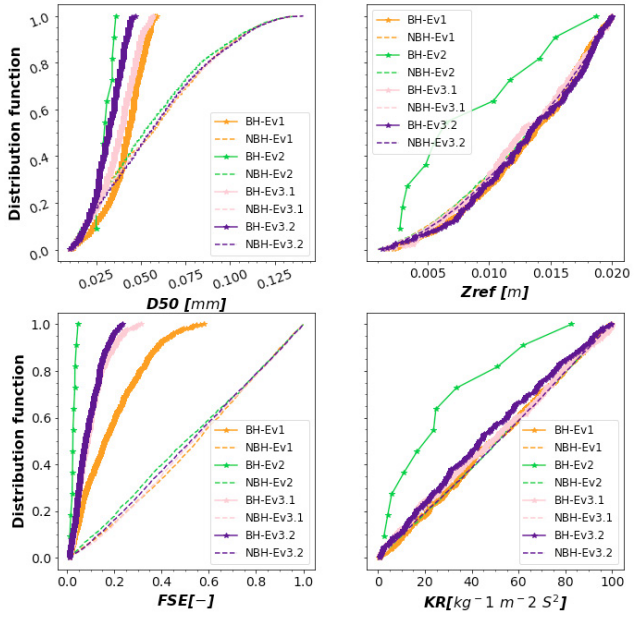

Figure 6. Posterior distributions for all the events and parameters: (top left) d_{50}, (top right) Z_{ref}, (bottom left) FSE, (bottom right) k_r (solid line: behavioral simulations, dashed line: non-behavioral simulations).

Fig. 6 shows the distributions for behavioral and non-behavioral simulation for all parameters and all flood events. Ev.2 has a different distribution than the other events but again, these results cannot be trusted because of the limited number of behavioral simulations. The distribution for other events are really similar for the most sensitive parameters FSE and d_{50} with a narrow range of behavioral simulations for these two parameters (Fig. 6). There is not any behavioral simulations for d_{50} higher than 0.06 mm. The distributions of FSE are very similar for the Ev.3.1 and Ev.3.2 with behavioral simulations for FSE values below 0.23 whereas it goes up to 0.58 for Ev.1. This corresponds to simulations with higher erosion rate which is consistent with the characteristics of Ev.1, which has a sediment peak above 30 g/L, i.e. almost 3 times higher than Ev.3 and 10 times higher than Ev.2 (Table 3).

As mentioned before, the efficiency of simulations is very sensitive to the coefficient corresponding to soil sensitivity to shear erosion FSE and the diameter of particles d_{50}. Only the lowest values of these both sensitive parameters result in behavioral simulations according to the chosen criterion.

The ranges of variation for the best simulation for each event are presented in Table 5. As expected, parameter variations of the best simulations for FSE and d_{50} are narrower compared to the chosen variation for Monte Carlo simulations (Table 1). Moreover, the values of FSE giving the ratio between effective and total stresses is of the order of 10% (Table 5: mean of 0.063 with a standard deviation of 0.04). This value is consistent with studies of sediment transport of different sizes and densities in the presence of vegetation (Le Bouteiller and Venditti, 2015; Romdhane et al., 2018). Similarly, the d_{50} value around 30 µm is also consistent with field observations which indicate an average diameter of 25 µm downstream of the catchment (Cea et al., 2016).

Table 5. Variation of each parameter for the best SSC simulation of each event (SD: Standard deviation)

Parameter	Min	Max	Mean	SD
d_{50} $[mm]$	0.0250	0.0330	0.0297	0.0030
Z_{ref} $[m]$	0.0013	0.0193	0.0101	0.0088
FSE [-]	0.022	0.101	0.063	0.041
k_r $[kg^{-1}.m^{-2}.s^2]$	0.52	50.96	11.94	19.75

4. CONCLUSIONS

Three flash flood events on the Cladueègne catchment are selected for performing the sensitivity analysis of soil erosion model using GSA-GLUE approach.

The most sensitive parameters are the coefficient of soil sensitivity to shear erosion FSE, and the median diameter of sediment particle d_{50}.

Results show the same trend for all event, with slightly different ranges of variation for the most sensitive parameter FSE in Ev.1 which presents the highest peaks of both discharge and SSC. Results cannot be trusted for Ev.2 due to the very low number of behavioral simulations which may be due either to poor sampling of the parameter space, or to excessive uncertainties in the observations of this event, or to an unsuitable model structure: further investigations are needed to conclude on this point. The different rainfall data in Ev.3 with different spatial variability leads to very different results in terms of hydrodynamics but similar results in terms of simulated SSC for Ev.3.1 and Ev.3.2 which needs to be investigated particularly in relationship with the actual location of the sediment sources. Uber (2020) also noted the importance of the effect of sediment sources on the hydrosedimentary response of this catchment.

The need to take into account the spatial variability of sediment sources is also highlighted by the fact that all best SSC simulations underestimates soil erosion.

Financial support: This work was carried out in the framework of the SedCrue project funded by the Région Occitanie / Pyrénées-Méditerranée and the Office Français de la Biodiversité (OFB).

REFERENCES

Adams, R., Western, A.W. and Seed, A.W. (2012). An analysis of the impact of spatial variability in rainfall on runoff and sediment predictions from a distributed model. Hydrological Processes, 26(21), pp. 3263–3280. https://doi.org/10.1002/hyp.8435.

Aksoy, H. and Kavvas, M.L. (2005). A review of hillslope and watershed scale erosion and sediment transport models. *CATENA*, 64(2–3), pp. 247–271. https://doi.org/10.1016/j.catena.2005.08.008.

Beven, K. and Binley, A. (1992). The future of distributed models: Model calibration and uncertainty prediction. *Hydrological Processes*, 6(3), pp. 279–298. https://doi.org/10.1002/hyp.3360060305.

Braud, I., et al. (2014). Multi-scale hydrometeorological observation and modelling for flash flood understanding. *Hydrol. Earth Syst*. Sci., 18, 3733–3761, https://doi.org/10.5194/hess-18-3733-2014.

Cea, L., Legout, C., Grangeon, T., and Nord, G. (2016). Impact of Model Simplifications on Soil Erosion Predictions: Application of the GLUE Methodology to a Distributed Event-Based Model at the Hillslope Scale. *Hydrological Processes*, 30(7), 1096-1113. https://doi.org/10.1002/hyp.10697.

Didon-Lescot, J.-F.; Ayral, P.-A.; Grard, N. (2015). OHM-CV mesures sur les Gardons. https://dx.doi.org/10.17180/OBS.OHM-CV.GARDONS.

Freer, J., Beven, K., Ambroise, B. (1996). Bayesian Estimation of Uncertainty in Runoff Prediction and the Value of Data: An Application of the GLUE Approach. *Water Resources Research*, 32(7), pp. 2161–2173. https://doi.org/10.1029/95WR03723.

Gaillardet, J. et al. (2018). OZCAR: The French Network of Critical Zone Observatories. *Vadose Zone Journal*, 17(1), p. 180067. https://doi.org/10.2136/vzj2018.04.0067.

Garambois, P.A., Roux, H., Larnier, K., Labat, D. and Dartus, D. (2015). Characterization of Catchment Behaviour and Rainfall Selection for Flash Flood Hydrological Model Calibration: Catchments of the Eastern Pyrenees. *Hydrological Sciences Journal*, 60(3), 424-47. https://doi.org/10.1080/02626667.2014.909596.

Hornberger, G.M., Spear, R.C. (1981). An approach to the preliminary analysis of environmental systems. *J. Environ. Manage*., 12(1), 7–18.

Kavetski, D., Kuczera, G., Franks, S.W. (2006). Bayesian analysis of input uncertainty in hydrological modeling: 1. Theory. *Water Resources Research*, 42(3). https://doi.org/10.1029/2005WR004368.

Kuczera, G. and Parent, E. (1998) Monte Carlo Assessment of Parameter Uncertainty in Conceptual Catchment Models: The Metropolis Algorithm. Journal of Hydrology, 211, 69-85. https://doi.org/10.1016/S0022-1694(98)00198-X.

Le Bouteiller, C., and Venditti, J. G. (2015). Sediment transport and shear stress partitioning in a vegetated flow, *Water Resources Research*, 51, https://doi.org/10.1002/2014WR015825.

Li, L., Xia, J., Xu, C.-Y. and Singh, V.P., (2010). Evaluation of the subjective factors of the GLUE method and comparison with the formal Bayesian method in uncertainty assessment of hydrological models. Journal of Hydrology, 390(3-4), 210-221. https://doi.org/10.1016/j.jhydrol.2010.06.044.

Merritt, W.S., Letcher, R.A., Jakeman, A.J. (2003). A review of erosion and sediment transport models. Environmental Modelling & Software, *The Modelling of Hydrologic Systems,* 18, 761–799. https://doi.org/10.1016/S1364-8152(03)00078-1.

Navratil, O., et al. (2011). Global uncertainty analysis of suspended sediment monitoring using turbidimeter in a small mountainous river catchment. *Journal of Hydrology*, 398, 246–259. https://doi.org/10.1016/j.jhydrol.2010.12.025.

Nord, G., et al. (2017). A High Space–Time Resolution Dataset Linking Meteorological Forcing and Hydro-Sedimentary Response in a Mesoscale Mediterranean Catchment (Auzon) of the Ardèche Region, France. *Earth System Science Data*, 9(1), 221-49. https://doi.org/10.5194/essd-9-221-2017.

Romdhane, H., Soualmia, A., Cassan, L. and Belaud, G. (2018). Effect of vegetation on flows and sediment transport, *E3S Web Conf.*, 40 02017. https://doi.org/10.1051/e3sconf/20184002017.

Roux, H., et al. (2011). A Physically-Based Parsimonious Hydrological Model for Flash Floods in Mediterranean Catchments. *Natural Hazards and Earth System Sciences*, 11(9), 2567-82. https://doi.org/10.5194/nhess-11-2567-2011.

Uber, M. (2020). Suspended Sediment Production and Transfer in Mesoscale Catchments: A New Approach Combining Flux Monitoring, Fingerprinting and Distributed Numerical Modeling. Phd Thesis, Université Grenoble Alpes. https://tel.archives-ouvertes.fr/tel-02926078.

Van Rijn, L. C. (1984). Sediment transport, part II: suspended load transport. *Journal of Hydraulic Engineering*, 110(11), 1613-1641.

Wagener, T., McIntyre, N., Lees, M.J., Wheater, H.S., Gupta, H.V. (2003). Towards reduced uncertainty in conceptual rainfall-runoff modelling: dynamic identifiability analysis. *Hydrological Processes* 17, 455–476. https://doi.org/10.1002/hyp.1135.

Wicks, J. M., and Bathurst, J. C. (1996). SHESED: A Physically Based, Distributed Erosion and Sediment Yield Component for the SHE Hydrological Modelling System. *Journal of Hydrology*, 175(1), 213-38. https://doi.org/10.1016/S0022-1694(96)80012-6.